# Observation of Multiple Charge Density Wave Phases in Epitaxial Monolayer 1T-VSe2 Film

**Junyu Zong**
Nanjing University
**Yang Xie**
Nanjing University
**Qinghao Meng**
Nanjing University
**Qichao Tian**
Nanjing University
**Wang Chen**
Nanjing University https://orcid.org/0000-0003-2174-5899
**Xuedong Xie**
Nanjing University
**Shaoen Jin**
Nanjing University
**Yongheng Zhang**
Nanjing University https://orcid.org/0000-0003-3716-4669
**Li Wang**
Suzhou Institute of Nano-tech and Nano-bionics
**Wei Ren**
Suzhou Institute of Nano-tech and Nano-bionics
**Jian Chen**
Suzhou Institute of Nano-Tech and Nano-Bionics (SINANO)
**Aixi Chen**
Suzhou Institute of Nano-tech and Nano-bionics
**Fangsen Li**
University of Science and Technology of China
**Zhaoyang Dong**
Nanjing University of Science and Technology
**Can Wang**
Nanjing University
**Jian-Xin Li**
Nanjing University
**Yi Zhang** ( zhangyi@nju.edu.cn )

Nanjing University https://orcid.org/0000-0003-1204-8717

**Article**

**Keywords:** 2D material, nanoscience, condensed-matter physics

**Posted Date:** May 19th, 2021

**DOI:** https://doi.org/10.21203/rs.3.rs-498840/v1

# Observation of Multiple Charge Density Wave Phases in Epitaxial Monolayer 1T-$VSe_2$ Film

Junyu Zong[1], Yang Xie[1], Qinghao Meng[1], Qichao Tian[1], Wang Chen[1], Xuedong Xie[1], Shaoen Jin[1], Yongheng Zhang[1], Li Wang[2], Wei Ren[2], Jian Chen[2], Aixi Chen[2], Fang-Sen Li[2], Zhaoyang Dong[3], Can Wang[1,4], Jian-Xin Li[1,4*], Yi Zhang[1,4†]

[1]*National Laboratory of Solid State Microstructure, School of Physics, Nanjing University, Nanjing, 210093, China*

[2]*Vacuum Interconnected Nanotech Workstation (Nano-X), Suzhou Institute of Nano-Tech and Nano-Bionics (SINANO), Chinese Academy of Sciences, Suzhou, 215123, China*

[3]*Department of Applied Physics, Nanjing University of Science and Technology, Nanjing 210094, China.*

[4]*Collaborative Innovation Center of Advanced Microstructures, Nanjing University, Nanjing, 210093, China*

Email: jxli@nju.edu.cn *

zhangyi@nju.edu.cn †

**Abstract**

**As a special order of electronic correlation induced by spatial modulation, the charge density wave (CDW) phenomena in condensed matters attract enormous research interests. Here, using scanning-tunneling microscopy in various temperatures, we observe a new (2×1) CDW phase besides the ($\sqrt{7}\times\sqrt{3}$) CDW phase in epitaxial monolayer 1T-$VSe_2$ film. Combining the variable-temperature angle-resolved photoemission spectroscopic (ARPES) measurements, we discover an anisotropic CDW gap and a two-step transition associated with the different CDW phases, which were observed below 135 K for the ($\sqrt{7}\times\sqrt{3}$) CDW phase and between 135 K to 330 K for the (2×1) CDW phase respectively. The ($\sqrt{7}\times\sqrt{3}$) CDW phase results a full gap, while the (2×1) CDW phase shows highly**

**momentum dependence and results a partial gap structure at the Fermi surface. This two-step transition with anisotropic gap opening and the resulted evolution in ARPES spectra are corroborated by our theoretical calculation based on a phenomenological form for the self-energy containing a two-gap structure. Our findings provide significant information and deep understanding on the CDW phases in monolayer 1T-$VSe_2$ film as a 2D material.**

In recent years, the discovery of plentiful two-dimensional (2D) materials brings new platform for studying novel phenomena in condensed matters[1-4]. Among the 2D materials family, transition metal chalcogenides (TMDCs) attract enormous research interests due to the abundant variety and properties[2-5]. For examples, the monolayer $NbSe_2$ and $FeSe_2$ were found to host superconductivity[6-8]; The monolayer 1T'-$WSe_2$ and 1T'-$WTe_2$ were found to be 2D topological insulators and exhibit quantum spin Hall effect[9,10]; The monolayer $TiSe_2$, $TaSe_2$ show CDWs with different orders[11,12], which became a typical research platform to understand the correlations between electrons and phonons[13-18]. Notably, $VSe_2$ was found to host various CDW phases. In bulk 1T-$VSe_2$, (4×4×3) CDW order has been observed below transition temperature $T_C$ = 110 K and its mechanism is suggested as 3D Fermi surface nesting[19-21], while the monolayer 1T-$VSe_2$ shows ($\sqrt{7}\times\sqrt{3}$) CDW order at low temperatures (< 4 K)[22]. Although CDWs are ubiquitous in some 3D and 2D materials, but the physical mechanism is still not received a unified explanation in $VSe_2$.

Using *in-situ* variable-temperature angle-resolved photoemission spectroscopic (VT-ARPES) and scanning-tunneling microscopic (STM) techniques, here we investigate the CDW phase transition in the monolayer 1T-$VSe_2$ film grown on bilayer graphene substrate by molecular beam epitaxial (MBE) method. We found a new CDW phase with (2×1) reconstruction undetected before, besides the ($\sqrt{7}\times\sqrt{3}$) reconstruction in the monolayer 1T-$VSe_2$. Through the analysis of the CDW gap evolutions at different momentum positions from the VT-ARPES spectra, we found that the CDW gap along

the *Γ-M* direction exhibits a monotonic temperature dependence and vanishes at 135 K, associated with the disappearance of the ($\sqrt{7}\times\sqrt{3}$) reconstruction observed by STM. Along the *M-K* direction, the CDW gap is also reduced with temperature, but does not vanish at 135 K, instead it extends to 330 K. Interestingly, the gap in the temperature range of 135 K-330 K coincides the (2×1) reconstruction detected by STM. Combining with the theoretical calculations using a phenomenological form for the self-energy containing a two-gap structure, we show that the CDW gap exhibits highly anisotropic momentum and temperature dependences, and shows a two-step transition along the *M-K* direction.

The monolayer 1T-$VSe_2$ film was grown on bilayer graphene substrate, which was obtained by flash annealing the 4H-SiC(0001) wafer at 1250 ℃ for 60 cycles [23]. The X-ray photoelectron spectroscopy (XPS), VT-ARPES and room-temperature scanning-tunneling microscopy (RT-STM) were performed *in-situ*. The ultra-low-temperature scanning-tunneling microscopy (ULT-STM) and variable-temperature scanning-tunneling microscopy (VT-STM) were performed *ex-situ* at Nano-X, Suzhou Institute of Nano-Tech and Nano-Bionics (SINANO), China. The first-principles calculations were performed using the QUANTUM ESPRESSO package base on density functional theory (DFT)[24]. The generalized gradient approximation with the Perdew-Burke-Ernzerhof functional[25] was used to describe the electron exchange and correlation effects. Detailed methods can be seen in the Supplementary Information.

The structure of the 1T-$VSe_2$ unit cell is represented as a ball and stick model in Figure 1(a). The triangle formed by the top layer of Se atoms is rotated by 180° relative to the bottom Se layer. The reflection high-energy electron diffraction (RHEED) image of a monolayer 1T-$VSe_2$ film grown on bilayer graphene substrate is shown in Figure 1(b). The sharp RHEED patterns prove that the film was well-crystalized. In Figure 1(c), the XPS spectrum shows the binding energies of Se $3d_{5/2}$ (~ 56 eV), Se $3d_{3/2}$ (~57 eV), V $2p_{3/2}$ (~ 512 eV) and V $2p_{1/2}$ (~ 520 eV) orbitals. To further determine the surface morphology of the sample, we took a 100×100 $nm^2$ STM image scanned at 7 K [Figure

1(d)]. The grown 1T-$VSe_2$ formed a large-scale flat single-layer film with a coverage of ~ 60%. Few bilayer islands were formed on the 1T-$VSe_2$ surface, but they will not affect our VT-ARPES and VT-STM measurements due to their rather small sizes. To determine the CDW order of the 1T-$VSe_2$ film in different temperature ranges, we took 4×4 $nm^2$ atom resolution images via ULT-STM at 7 K [Figure 1(e)], VT-STM at 150 K [Figure 1(f)], and RT-STM at 300 K [Figure 1(g)], respectively. A clear ($\sqrt{7}\times\sqrt{3}$) CDW phase marked by the red arrows was clearly observed at 7 K [Figure 1(e)]. This CDW order is consistent with previous reports[22,26,27]. At 150 K, we can observe a very clear stripe structure, and the reconstruction vectors marked by the red arrows show a (2×1) CDW phase [Figure 1(f)]. Notably, this (2×1) CDW phase in monolayer 1T-$VSe_2$ has not been reported yet. When the temperature rises to 300 K, only the (1×1) pure atom-resolved image can be observed, and no CDW reconstruction was found [Figure 1(g)], which means that the CDW phases are destructed thermally when temperature is above 300 K through STM measurements.

To unveil the physical properties of the ($\sqrt{7}\times\sqrt{3}$) and (2×1) CDW phases at different temperature ranges, we performed VT-APRES measurements to study the entire energy band structures and CDW gap evolutions of the monolayer 1T-$VSe_2$ film at various temperatures. Figure 2(a) shows the constant-energy-mapping at binding energy of -0.1 eV below the Fermi level at a temperature of 7 K. Six oval pockets can be observed around the six M points of the hexagonal Brillouin zone (BZ), which is consistent with the calculated Fermi surface from the previous reports[28-30]. Figure 2(b) shows the ARPES spectra along the *Γ-M-K* directions. We can see that the band disperses towards the Fermi level at the momentum positions marked by red and blue arrows, at which the CDW gaps can be observed and extracted from the energy distribution curves (EDCs) of the ARPES spectra. Figures 2(c) and 2(d) show the symmetrized EDCs with subtraction of Fermi function at the momentum positions marked by the red and blue arrows, respectively. These EDCs were taken at temperatures from 7 K to 340 K. The peaks on the symmetrized EDCs are the occupied states, and as usual we take the distance between the two peaks to be twice the CDW

gap (2×Δ). When the temperature rises, the peaks of the EDC will gradually flatten around the 0 eV, which means that the EDC gap closes. The temperature dependence of the CDWs gaps extracted from Figures 2(c) and 2(d) were plotted in Figures 2(e) and 2(f). Remarkably, we found that the gaps at different momentum positions show quite distinct behaviors. At the momentum position marked by the red arrow near the $\Gamma$ point, the CDW gap exhibits a monotonic temperature dependence and gradually decreases from 31±5 meV to zero at ~ 135 K; while at the momentum position marked by the blue arrow, the CDW gap decreases from 62±5 meV to 31±12 meV at ~ 135 K, then it shows a stable decrease with temperature in an extended range and finally drops to zero at ~ 330K.

According to our above STM results, one may ascribe the low temperature gap as resulting from the ($\sqrt{7}\times\sqrt{3}$) CDW phase, while the intermediate temperature gap as that due to the (2×1) CDW phase. Therefore, we suggest a two-gap formula at the mean-field level[22] to describe the temperature dependence of the CDW gap,

$$\Delta_i(T) \propto \tanh\left(A\sqrt{\frac{T_{Ci}}{T}-1}\right)\Theta(T_{Ci}-T),\ i=1,2, \quad (1)$$

where $A$ = 1.2 is a proportional constant and Θ is the unit step function. At the momentum position marked by the red arrow near the Γ point, only $\Delta_1$ is included. The fitting results to the experimental data are shown in Figure 2(e) as the red line. It shows a well agreement to the original data. According to the fitting result, we get $\Delta_1$ = 31±3 meV, $T_{C1}$ = 135±10 K. At the momentum position marked by the blue arrow near the M point, both $\Delta_1$ and $\Delta_2$ are included, and we use $\Delta_1$(T)+$\Delta_2$(T) to fit the data shown as the red line in Figure 2(f), we get a very good fitting result with $\Delta_2$ = 31±3 meV and $T_{C2}$ = 330±10 K. The combination of the experimental results and the theoretical fitting indicates that there exist two distinct CDW gaps with highly anisotropic gap distributions in the momentum space, in particular a two-step gap transition along the *M*-*K* direction in the monolayer 1T-$VSe_2$, one is associated with the ($\sqrt{7}\times\sqrt{3}$) CDW with a transition temperature of ~ 135 K (denoted by $\Delta_1$), while another

is associated with the (2×1) CDW with a transition temperature of ~ 330 K (denoted by $\Delta_2$). Notably, the $\Delta_2$ shows a highly anisotropic momentum dependence, which has no trance near the $\Gamma$ point but can be clearly observed near the $M$ point.

With the two-gap form, we can go further to make a comparison to the experimental ARPES spectra by using the phenomenological self-energy expression[31] developed originally for high-Tc cuprates,

$$\Sigma(\mathbf{k},\omega) = -i\Gamma_1 + \frac{\Delta i^2}{[\omega+\epsilon(\mathbf{k})+i\Gamma_0]}, \quad (2)$$

where $\Delta i$ is the CDW gap, $\Gamma_1$ the single-particle scattering rate, $\Gamma_0$ the inverse particle-hole pair lifetime, and $\epsilon(\mathbf{k})$ the single-particle dispersion. Using Eq. (2), we can calculate the single-particle spectral function $A(\mathbf{k},\omega)$ via the Green's function as $\mathrm{A}(\mathbf{k},\omega) = -\mathrm{ImG}(\mathbf{k},\omega)/\pi$ with $\mathrm{G}(\mathbf{k},\omega) = [\omega - \epsilon(\mathbf{k}) - \Sigma(\mathbf{k},\omega)]^{-1}$. In our numerical calculations, $\epsilon(\mathbf{k})$ is obtained by the tight-binding fit to the first-principles calculations for 1T-$VSe_2$, and $\Gamma_1$ = 0.005 and $\Gamma_0$ = 0.005 are chosen. Figures 3(a)-3(c) show the calculated spectral functions along the $M$-$\Gamma$-$M$ and $K$-$M$-$K$ directions at 340 K, 200 K and 7 K, respectively. Figures 3(d)-3(f) are the corresponding experimental data. The calculated spectra show a good agreement to the experimental results. At 340 K, both the $\Delta_1$ and $\Delta_2$ equal to zero according to Eq. (1), and the calculated spectra function and ARPES spectra show no gap along both $\Gamma$-$M$ and $M$-$K$ directions [Figure 3(a) and 3(d)]. When temperature is reduced to be 200 K, $\Delta_1$ keeps zero but $\Delta_2$ becomes nonzero. Since $\Delta_2$ only exists along the $M$-$K$ direction, the band along the $M$-$K$ direction opens a small gap at Fermi level but the band along the $\Gamma$-$M$ direction still shows no gap [Figure 3(b) and 3(e)]. When temperature is further reduced to be 7 K, both $\Delta_1$ and $\Delta_2$ becomes nonzero. Since $\Delta_1$ exists in both the $\Gamma$-$M$ and $M$-$K$ directions while $\Delta_2$ not, thus the band along the $M$-$K$ direction shows a larger gap than that along the $\Gamma$-$M$ direction at the Fermi level [Figure 3(c) and 3(f)]. Due to the existence of the CDW gap, the band near the Fermi level is bent, which can also be seen in the secondary differential spectra along the $M$-$\Gamma$-$M$ direction as shown in the Supplementary Information [see Figure S1]. In addition, the shape of the constant energy mapping is also modified.

We note that by simply treating the scattering rates $\Gamma_1$ and $\Gamma_0$ as constants in our calculations using Eq. (2), we get a good agreement to the experimental data. It suggests that the single-particle scattering rate $\Gamma_1$ and inverse pair lifetime $\Gamma_0$ may show less or even no temperature dependence, and also affect less the CDW phase transitions and gap evolutions in monolayer 1T-$VSe_2$. This is in contrast to the case in high-Tc cuprates[31], where both $\Gamma_1$ and $\Gamma_0$ assumes a strong temperature dependence.

In summary, we found a new (2×1) CDW phase in the temperature range between 135 K to 330 K besides the ($\sqrt{7}\times\sqrt{3}$) CDW phase existing below 135 K in the epitaxial monolayer 1T-$VSe_2$ film. Combining our theoretical analysis, we found that these two CDW phases exhibit a two-step CDW gap transition. The one corresponding to the ($\sqrt{7}\times\sqrt{3}$) reconstruction results a full gap. While the other corresponding to the (2×1) reconstruction shows a highly momentum dependence and results a partial gap structure at the Fermi surface. Our results illustrate an unusual CDW phenomenon in monolayer 1T-$VSe_2$.

**Acknowledgments**

This work is supported by the National Natural Science Foundation of China (Grant Nos. 11774154, 11790311, 12004172, 11774152，11604366，11634007), the National Key Research and Development Program of China (No. 2018YFA0306800, 2016YFA0300401), the Program of High-Level Entrepreneurial and Innovative Talents Introduction of Jiangsu Province, the Jiangsu Planned Projects for Postdoctoral Research Funds (Grant No. 2020Z172) and Natural Science Foundation of Jiangsu Province (No. BK 20160397).

**Conflict of Interest**

The authors declare no conflict of interest.

**REFERENCE**


1 Khan, K. *et al.* Recent developments in emerging two-dimensional materials and their applications. *Journal of Materials Chemistry C* **8**, 387-440 (2020).

2 Barja, S. *et al.* Charge density wave order in 1D mirror twin boundaries of single-layer $MoSe_2$. *Nat Phys* **12**, 751-756 (2016).

3 Deng, Y. *et al.* Quantum anomalous Hall effect in intrinsic magnetic topological insulator $MnBi_2Te_4$. *Science* **367**, 895-900 (2020).

4 Yang, L. X. *et al.* Weyl semimetal phase in the non-centrosymmetric compound TaAs. *Nat Phys* **11**, 728-+ (2015).

5 Manzeli, S., Ovchinnikov, D., Pasquier, D., Yazyev, O. V. & Kis, A. 2D transition metal dichalcogenides. *Nature Reviews Materials* **2**, 17033 (2017).

6 He, S. L. *et al.* Phase diagram and electronic indication of high-temperature superconductivity at 65 K in single-layer FeSe films. *Nat Mater* **12**, 605-610 (2013).

7 Xi, X. X. *et al.* Ising pairing in superconducting $NbSe_2$ atomic layers. *Nat Phys* **12**, 139-+ (2016).

8 Wang, Q.-Y. *et al.* Interface-Induced High-Temperature Superconductivity in Single Unit-Cell FeSe Films on $SrTiO_3$. *Chinese Physics Letters* **29**, 037402 (2012).

9 Pedramrazi, Z. *et al.* Manipulating Topological Domain Boundaries in the Single-Layer Quantum Spin Hall Insulator 1T'-$WSe_2$. *Nano Letters* **19**, 5634-5639 (2019).

10 Tang, S. J. *et al.* Quantum spin Hall state in monolayer 1T'-$WTe_2$. *Nat Phys* **13**, 683-+ (2017).

11 Chen, P. *et al.* Charge density wave transition in single-layer titanium diselenide. *Nature communications* **6**, 8943 (2015).

12 Ryu, H. *et al.* Persistent Charge-Density-Wave Order in Single-Layer $TaSe_2$. *Nano Letters* **19**, 626-626 (2019).

13 Xi, X. X. *et al.* Strongly enhanced charge-density-wave order in monolayer $NbSe_2$. *Nat Nanotechnol* **10**, 765-+ (2015).

14 Campi, D., Bernasconi, M. & Benedek, G. Phonons and electron-phonon interaction at the Sb(111) surface. *Phys Rev B* **86**, 075446 (2012).

15 Yu, S. J., Zhang, J. T., Tang, Y. & Ouyang, M. Engineering Acoustic Phonons and Electron-Phonon Coupling by the Nanoscale Interface. *Nano Letters* **15**, 6282-6288 (2015).

16 Lee, H. A Theoretical Model of Thermoelectric Transport Properties for

Electrons and Phonons. *J Electron Mater* **45**, 1115-1141 (2016).

17 Rossnagel, K. On the origin of charge-density waves in select layered transition-metal dichalcogenides. *Journal Physics Condensed Matter* **23**, 213001 (2011).

18 Chen, C. W., Choe, J. & Morosan, E. Charge density waves in strongly correlated electron systems. *Reports Progress Physics* **79**, 084505 (2016).

19 Eaglesham, D. J., Withers, R. L. & Bird, D. M. Charge-Density-Wave Transitions in 1T-$Vse_2$. *J Phys C Solid State* **19**, 359-367 (1986).

20 Jolie, W. *et al.* Charge density wave phase of $VSe_2$ revisited. *Phys Rev B* **99**, 115417 (2019).

21 Strocov, V. N. *et al.* Three-dimensional electron realm in VSe2 by soft-x-ray photoelectron spectroscopy: origin of charge-density waves. *Physical Review Letters* **109**, 086401 (2012).

22 Chen, P. *et al.* Unique Gap Structure and Symmetry of the Charge Density Wave in Single-Layer $VSe_2$. *Physical Review Letters* **121**, 196402 (2018).

23 Wang, Q. *et al.* Large-scale uniform bilayer graphene prepared by vacuum graphitization of 6H-SiC(0001) substrates. *Journal of Physics: Condensed Matter* **25**, 095002 (2013).

24 Giannozzi, P. *et al.* QUANTUM ESPRESSO: a modular and open-source software project for quantum simulations of materials. *Journal of Physics: Condensed Matter* **21**, 395502 (2009).

25 Perdew, J. P., Burke, K. & Ernzerhof, M. Generalized gradient approximation made simple. *Physical Review Letters* **77**, 3865-3868 (1996).

26 Feng, J. G. *et al.* Electronic Structure and Enhanced Charge-Density Wave Order of Monolayer $VSe_2$. *Nano Letters* **18**, 4493-4499 (2018).

27 Duvjir, G. *et al.* Emergence of a Metal-Insulator Transition and High-Temperature Charge-Density Waves in $VSe_2$ at the Monolayer Limit. *Nano Letters* **18**, 5432-5438 (2018).

28 Cudazzo, P., Gatti, M. & Rubio, A. Interplay between structure and electronic properties of layered transition-metal dichalcogenides: Comparing the loss function of 1T and 2H polymorphs. *Phys Rev B* **90**, 205128 (2014).

29 Esters, M., Hennig, R. G. & Johnson, D. C. Dynamic instabilities in strongly correlated $VSe_2$ monolayers and bilayers. *Phys Rev B* **96**, 235147 (2017).

30 Jang, I. *et al.* Universal renormalization group flow toward perfect Fermi-surface nesting driven by enhanced electron-electron correlations in monolayer vanadium diselenide. *Phys Rev B* **99**, 014106 (2019).

31 Norman, M. R., Randeira, M., Ding, H. & Campuzano, J. C. Phenomenology of the low-energy spectral function in high-T-c superconductors. *Phys Rev B* **57**,

R11093-R11096 (1998).

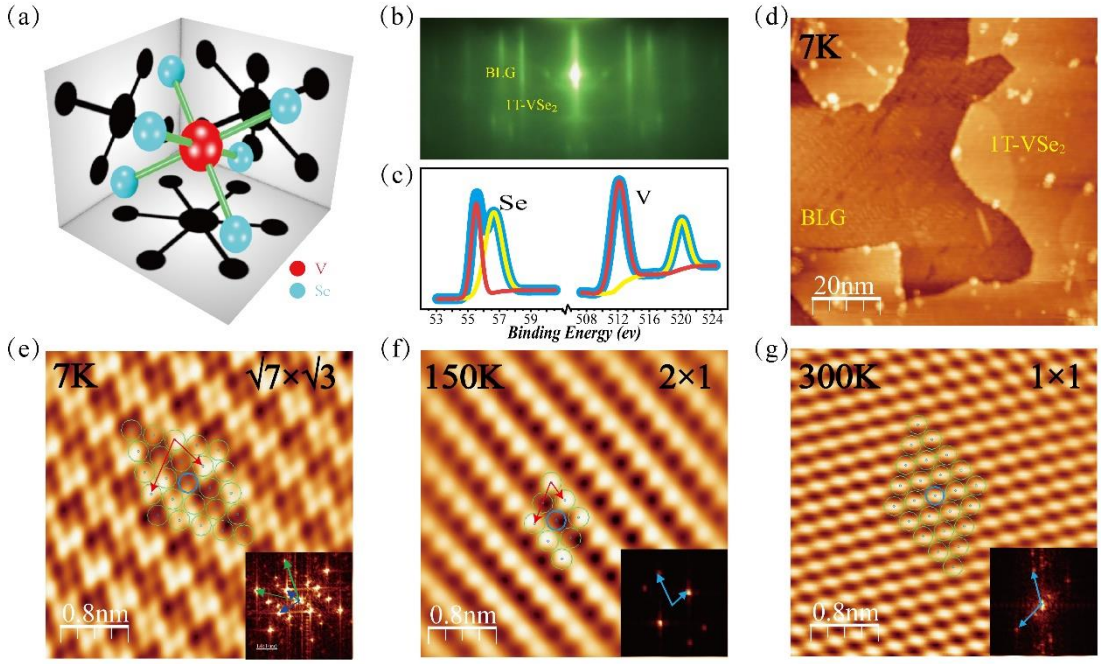


**FIG. 1. Unit cell structure, RHEED, XPS, and STM images of monolayer 1T-Vse2.** **(a)** The structure of the 1T-$VSe_2$unit cell. **(b) and (c)** RHEED pattern and XPS spectrum of monolayer 1T-$VSe_2$ grown on bilayer graphene substrate. **(d)** STM image (100×100 $nm^2$) scanned at 7 K. The bilayer graphene substrate and monolayer 1T-$VSe_2$ film are marked by yellow texts. **(e)** The atomic resolution STM image (4×4 $nm^2$) obtained at 7 K, and the reconstruction vectors of the ($\sqrt{7}\times\sqrt{3}$) CDW phase are marked by the red arrows. **(f)** The atomic resolution STM image (4×4 $nm^2$) obtained at 150 K, and the reconstruction vectors of (2×1) CDW phase are marked by the red arrows. **(g)** The STM image (4×4 $nm^2$) scanned at room-temperature (300 K).

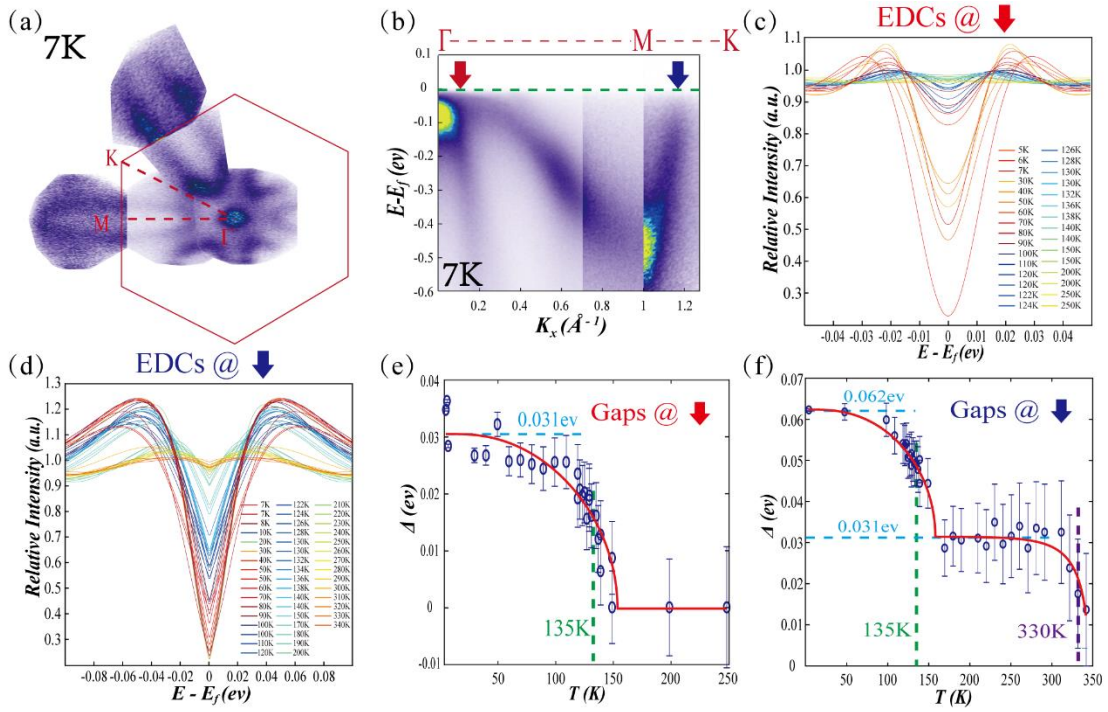


**FIG. 2. ARPES spectra and CDW gaps of monolayer 1T-$VSe_2$ film. (a)** BZ and constant energy mapping of monolayer 1T-$VSe_2$ at binding energy of -0.1 eV taken at 7 K. **(b)** ARPES spectra along the *Γ-M-K* direction taken at 7 K. **(c) and (d)** Symmetric EDCs at different temperatures at the momentum position marked by the red and blue arrow in (b), respectively. The different temperatures are marked by different line colors. **(e)**Temperature dependence of the CDW gap extracted from the EDCs at the momentum position marked by the red arrow. The red line are the fitting results from Eq. (1) using single $\Delta_1$. The blue and red dashed lines indicate the fitting results of $\Delta_1$ = 31 meV and $T_{C1}$ =135 K, respectively. **(f)** Temperature dependence of the CDW gap extracted from the EDCs at the momentum position marked by the blue arrow. The red line are the fitting results from Eq. (1) using total $\Delta(T)=\Delta_1(T)+\Delta_2(T)$. The blue dashed lines indicate the fitting results of $\Delta_1 = 31$ meV and $\Delta_1+\Delta_2 = 62$ meV, and the green and purple dashed lines indicate the fitting results of $T_{C1}$ = 135 K and $T_{C2}$ = 330K, respectively.

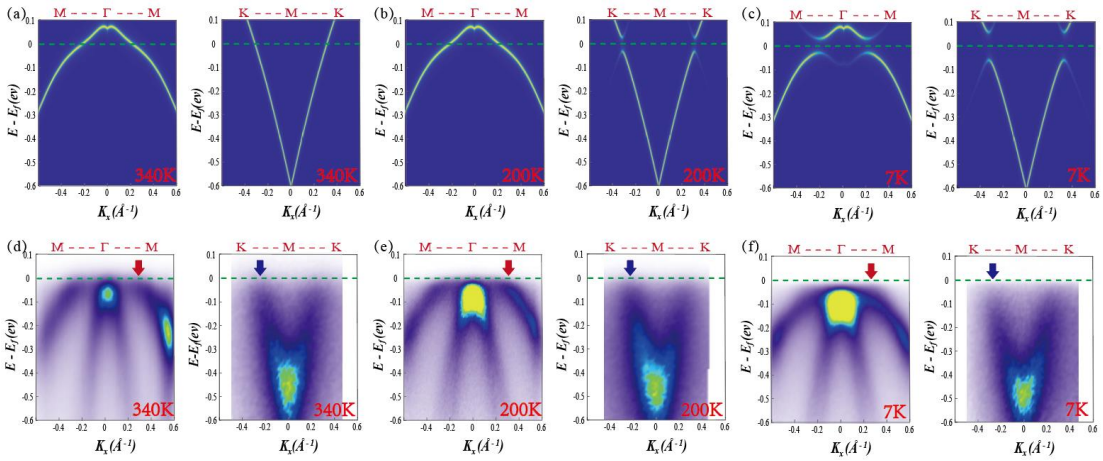


**FIG. 3. Comparison of theoretical calculations and ARPES spectra. (a)-(c)** Calculated spectral function at selected temperatures along the *M-Γ-M* and *K-M-K* directions. **(d)-(f)** ARPES spectra along the *M-Γ-M* and *K-M-K* directions scanned at the corresponding temperatures experimentally.

## Supplementary Files

This is a list of supplementary files associated with this preprint. Click to download.

- SIofCDWinVSe2.pdf